Radiation Characterization and Mitigation of High Energy H+ Beams

Peter DeRosa, Wilhelm Platow, Kevin Wenzel

Axcelis Technologies, 108 Cherry Hill Drive, Beverly, Massachusetts, USA, peter.derosa@axcelis.com

1. Abstract

High energy proton implants are used in the manufacturing process of IGBT devices to improve performance by extending minority carrier lifetime and reducing switching speeds. The energy requirement for H+ implanted into these devices exceeds the nuclear fusion reaction threshold above 300 keV of beamline liners containing ^{12}C, ^{13}C, and ^{29}Si within silicon wafers of the ion implant systems. The prompt γ-ray photon radiation generated from $^{12}C(p, \gamma)^{13}N$ and $^{29}Si(p, \gamma)^{30}P$ reactions have been characterized using a photon energy resolving Sodium-Iodide (NaI) scintillating crystal detection system. Determination of the photon energy is instrumental for designing a precise shielding system that can prevent exposure to ionizing radiation. Dosimetry results are reported to characterize the radiation emitted from post-implant Si wafers given the $^{29}Si(p, \gamma)^{30}P$ reaction, radiation emitted from post-implant SiC wafers given the $^{12}C(p,\gamma)^{13}N$ reaction, and the radiation present from the graphite beamline liners compared to high-Z mitigative liners.

2. Introduction

Proton induced nuclear reactions occur once the energy of the incoming beam exceeds the needed energy to overcome the coulomb barrier of the target nucleus. A direct nuclear collision, where the impact parameter of the beam is less than the nuclear radius of the target, will then cause fusion with the target nucleus and beam projectile to form a compound nucleus with excitation energy E_x. The relation between the proton energy E_p and the excitation energy E_x of a (p,γ) nuclear resonance is given by:

$$E_x = \left[\left(m_T + m_p\right) - m_C\right]c^2 + \frac{m_T}{m_T+m_p}E_p \frac{2}{1+\sqrt{1+2E_p m_T/(m_T+m_p)^2 c^2}} \qquad (1)$$

Where m_T, m_p, m_C is the target nuclei, proton, and compound nucleus mass respectively [4]. If E_x exceeds the separation energy of a nucleon from the compound nucleus, a proton, neutron, or alpha particle will decay off the compound nucleus. Once the compound nucleus is below nucleonic separation energy, γ-ray photon emission will shed the remaining E_x to the ground state. γ-ray photons are the result

of nucleons transitioning within the nucleus, analogous to electrons transitioning within electron orbitals releasing x-rays. The γ-ray photon transition probability λ is given by Fermi's golden rule:

$$\lambda = \frac{2\pi}{\hbar} |V_{fi}|^2 \, p(E_f) \quad (2)$$

Where $|V_{fi}|^2$ is the transition matrix element that relates the final and initial states of the transition, and $p(E_f)$ is the density of final nuclear states. Transition probability correlates to the wavefunction overlap of initial and final states. The compound nucleus now will either remain stable or beta-decay to a more stable isotope (see Fig. 1d) on the isobar mass parabola. The reactions explored in this work are namely proton capture nuclear fusion reactions, where the resulting E_x does not exceed the nucleonic separation threshold, resulting in the decay modes for the compound nucleus being γ-ray photon emission followed by beta-decay if the compound is not a stable isotope [3].

Beamline material and wafer implant irradiation studies were performed using H^+ beams up to 1.9 MeV and 1000 pμA. Direct measurement of γ-ray photon emissions is traditionally done using dosimetry to regard radiation safety, and γ-ray spectroscopy where the energy of the γ-ray photons is resolved in a crystal detector. Dosimetry experiments were conducted by bombarding H^+ ions into thick faraday targets within the endstation of an Axcelis ion implanter, with detector systems outside of the vacuum chamber walls (see Fig. 1c). γ-ray photon spectroscopy was performed using a 81 x 127 x 407mm Sodium Iodide (NaI) crystal spectrometer. Processed using an Osprey digitizer utilizing Digital Pulse Processing - Pulse Height Analysis (DPP-PHA), and spectral analysis done in ROOT C++ [6]. This system gives direct confirmation of each nuclear reaction taking place, resolving the photon radiation's kinetic energy, which can be used to calculate the efficiency of Pb shielding. Wafer radioactivity data was extracted using FLUKE handheld photon dosimeters, placed atop of the FOUP and measured the decaying radiation of isotopes post implant (see Fig. 3c). Each detection method will be explored for several carbon and silicon isotopes present in the ion implantation system.

3. Prompt Radiation Dosimetry

Operation of a H^+ beam with a graphite lined beamline above E_p = 457 keV will promote the $^{12}C(p, \gamma)^{13}N$ reaction via a nuclear resonance. This produces notable radiation fields at 50 cm from the H^+ beam strike point (see Fig. 1a). There are two reactions within graphite: $^{12}C(p,\gamma)^{13}N$ and $^{13}C(p, \gamma)^{14}N$ that have resonances produced starting at E_p = 457 and 550 keV respectively [1]. Thes are the cause of the

sharp increase of radiation right after 450 keV for the graphite data in Fig. 1a. With a scanned beam, the density of nuclear reactions is spread out effectively decreasing the near field radiation levels. The effect of distance is described by the inverse square of law, where this effect leads to a decrease in dose rate by 20%. Once an implant is complete, the β^+ decay of ^{13}N from the graphite target is visible post implant (see Fig 1b). For our experiment, the next implant started after 1900 seconds, with a brief use of spot beam during beam tuning before implant.

The intensity of the radiation resultant from proton induced nuclear reactions shows that graphite produces much higher dose rates compared to high-Z substitute liner. This is because the beam energy requirement for fusion with a proton beam for high-Z materials is dramatically increased. The high-Z radiation in Fig. 1a presents an about 10X decrease in dose rate compared to the graphite radiation. The radiation emission mechanism is different for the high-Z data compared to the proton induced fusion reaction with graphite. The high-Z radiation observed is characteristic to that of inelastic coulomb scattering referred as coulomb excitation instead of proton induced fusion, where the proton beam does not have enough energy for direct nuclear collision to occur. However, the beam transfers kinetic energy to the target nucleus, where the maximum available excitation energy given to the target nucleus is the kinetic energy of the beam, promoting the target nucleus into an excited state configuration. This mechanism shows a decreased production of photons when compared to the fusion reaction produced from graphite at the same energy via dosimetry in Fig. 1 [3].

4. γ-ray Photon Spectroscopy Analysis

γ-ray photon spectroscopy allows for the energy of the incoming radiation to be resolved by introducing a crystal medium in the path of the radiation (See Knoll for detection physics [2]). Once a photon enters the crystal detector, the probability of the full energy of the photon stopping in the detector goes down as the photon energy increases. To model this, GEANT4 is used to determine the theoretical detection efficiency as a function of energy. The energy spectrum can be calibrated using known sources with known photon emission energies such as ^{60}Co, ^{152}Eu, or ^{137}Cs. Utilization of ROOT C++ [6] provides 1D histograms of photon spectra seen in Fig. 2.

In Fig. 2, each of the three photon energy spectra were captured using a NaI scintillation detector with an energy resolution of 8.5 ± 0.8 % at 662 keV. Each of the three spectra resultant from the graphite

irradiation are background subtracted and normalized to be equivalent run times. The 1.9 MeV graphite spectra compared to 1.6 and 1.4 MeV shows evidence of a higher lying excited state in ^{14}N, which released a 3378 keV photon. Secondary photon interactions within the NaI crystal are visible in spectra such as Compton scattering, and escape peaks caused from pair production. At 7966 keV, pair production is almost completely dominant in this energy region for photons. This is seen as escape peaks, the photon (of energy greater than twice the rest mass of an electron) comes into the detector and creates a positron electron annihilation pair. The E_γ= 511 keV and E_γ =1022 keV peaks are distinguished [2]. For, Si bombarded with protons at 1.9 MeV (Fig. 2c) it is shown that all 3 stable isotopes of Si can undergo fusion reactions with a proton beam.

Utilizing calibrated γ-ray energy spectra in Fig 2, allows for the identification of emitted photons to an excited state configuration of nucleons of a singular isotope. Level schemes are a nuclear physicist's way of organizing a nucleus as it de-excites to its fermi configuration. The photon's electromagnetic and quantum mechanical properties can be determined if the initial and final state properties are known. Coincidence measurements were not conducted in this work to assign γ-ray transitions; however, assignment was done based on target isotopic abundance and visible photon intensity. The observed γ-ray transition scheme of each decay scheme for ^{14}N, ^{13}N, ^{31}P, and ^{30}P (Fig. 3 a,b,c,d), reflects that the maximum excitation energy of these nucleonic configurations did not exceed the calculated E_x value of the fusion reactions. Each of the detected γ-ray photon energies and excited state assignments have been previously studied using similar nuclear reaction mechanisms, with the γ-rays detected acting as a fingerprint for each product nucleus.

Finally, by extracting the photon energies, a complete understanding of the shielding efficiency of each photon contribution can made. In Fig. 3E, 10 mm of Pb applied at 50 cm results in a shielding efficiency ranging from 81.5 – 89.1 % given the photon energy of 7964 – 898 keV, respectively.

5. Post Proton Implantation - Radioactive Decay

Proton induced fusion with carbon and silicon (^{12}C(p,γ)^{13}N and ^{29}Si(p,γ)^{30}P) with confirmation of these nuclear reactions via Fig. 2 and Fig. 3, leaves ^{13}N and ^{30}P as unstable fusion products. These nuclei formed within the graphite liners or within a Si wafer and subsequently β^+ decay to a stable isotope. The decaying radiation emits 511 keV γ-rays due to positron annihilation. Fig. 4 shows the radiation field

intensity post implant for different wafer types.

Direct measurement of the decay curves from 1.1, 1.6 and 1.9 MeV proton implants into bare Si yield experimental half-lives of 171.9 ± 13.1, 163.6 ± 12.8, and 169.1 ± 13.0 seconds, respectively. The literature value of ^{30}P half-life is 150 seconds [1]. The relative radiation intensity increases by 250% between 1.1 and 1.9 MeV proton implants given the same wafer dose and beam current. With different Si wafer types, it was found that no change in intensity between wafer types over an increasing wafer dose from 10^{15} to $5x10^{15}$ ions/cm^2. The activation radiation from Si and doped Si wafers is namely caused from the β^+ decay of ^{30}P. For SiC however, at 600 keV, the isotopic contents of ^{12}C and ^{29}Si become activated. The radiation waveform's intensity is dominated by the ^{13}N decay over the ^{30}P. The literature half-life for ^{13}N is 598.02 seconds [1].

6. Conclusion

γ-rays photon dosimetry and spectroscopy experiments were performed using H^+ beams to illuminate the nuclear radiation mechanisms present during proton beam strike with beamline materials, Si, and SiC wafer implantation. Leveraging this spectroscopic method, a tailored radiation Pb shielding scheme was determined for safety of operation such that the prompt photon radiation during implantation can be mitigated by changing the beamline liners to a high-Z material and applying Pb shielding. Proton induced fusion reactions were identified and characterized for $^{12}C(p,\gamma)^{13}N$, $^{13}C(p,\gamma)^{14}N$, 29Si(p,γ)30P and 30Si(p,γ)31P reactions. These transition schemes illuminate the entire radiation process during and after implantation.

After the H^+ beam is removed from the target materials, there is subsequent decaying radiation due to β^+ emission from ^{13}N and ^{30}P formed from proton induced fusion. Decaying radiation produced from H+ implanted into bare Si wafers is solely resultant from the β^+ decay of ^{30}P. Production of ^{30}P possesses the biggest safety concern post-implant for bare Si wafers, however all three stable isotopes of Si are resolvable from prompt radiation via γ-ray spectroscopy. Analysis of H^+ beam induced SiC decay radiation shows that ^{13}N is the dominant activation responsible for most of the radiation intensity visible via dhtfhtfyu6osimetry. The dominant radiation intensity resulting from H^+ implants is mainly caused from bulk concentrations of common beamline and wafer substrate materials given the relative nuclear cross sections.

7. Acknowledgment

The Authors would like to thank Guang Mo and Ron Lessard at Axcelis for their equipment engineering support in the operation of the beams used for experiments presented in this work.

8. Conflict of Interest

No funds, grants, or other support was received.

9. Data Availability Statement

The datasets used in the analysis of this work are available from the corresponding author under reasonable request.

References

[1] *US Department of Energy, BNL. Nation Nuclear Data Center.*

[2] G.F. Knoll. *Radiation Detection and Measurement.* John Wiley & Sons, 2010. ISBN:978-0-470-13148-0.

[3] Kenneth S. Krane. Introductory Nuclear Physics. John Wiley & Sons, 1988. ISBN: 0-471-80553-X.

[4] Kikstra, S. W. (n.d.). *Proton capture reactions and nuclear structure*. https://inis.iaea.org/collection/NCLCollectionStore/_Public/21/041/21041960.pdf

[5] Geant4 - A Simulation Toolkit, S. Agostinelli et al., Nucl. Instrum. Meth. A 506 (2003) 250-303

[6] Rene Brun and Fons Rademakers, ROOT - An Object Oriented Data Analysis Framework, Proceedings AIHENP'96 Workshop, Lausanne, Sep. 1996, Nucl. Inst. & Meth. in Phys. Res. A 389 (1997) 81-86.

FIGURES:

Fig. 1 : (**a**) Photon dosimetry of graphite and high-Z targets at 1000 pμA H^+ beam varying energy E_p = 200 to 1900 keV measured 50 cm from target. (**b**) Time dependent photon dosimetry during 10^{15} ions/cm^2 1.1 MeV 1000 pμA H^+ implants into Si wafers. (**c**) Experimental setup. H^+ beam injected into the Axcelis process chamber where the faraday plate exhibits beam strike. (**d**) Proton induced fusion with ^{12}C forming a compound nucleus of ^{13}N, followed by γ-ray photon emission, and finally the β^+ decay to stable ^{13}C

Fig. 2 : γ-ray spectroscopy for H^+ into C and Si using a 76 x 127 x 407 mm NaI detector at 30cm. (**a**) γ-ray spectra of H^+ into a carbon thick target. Photon energy range from 800 keV to 3700 keV. H^+ Energy

varied from 1.9, 1.6, and 1.4 MeV at 1000uA. (**b**) γ-ray spectra of H^+ into a carbon thick target. Photon energy range from 3700 keV to 8000 keV H^+. (**b**) γ-ray spectra of 1.9 MeV H^+ into a N-type Si wafer, photon energy ranges from 800 keV to 5000 keV.

Fig. 3: Nuclear excitation level schemes of visible photon intensities. E_x is calculated from Eq. (1) using E_p = 1.9 MeV, with J^π and energy values of excited states extracted from NNDC [1]. (**a**) Observed nuclear structure of $^{13}C(p,\gamma)^{14}N$, $E_x = 9.323\ MeV$. (**b**) Observed nuclear structure of $^{12}C(p,\gamma)^{13}N$, $E_x = 3.710\ MeV$. (**c**) Observed nuclear structure of $^{30}Si(p,\gamma)^{31}P$, $E_x = 9.149\ MeV$. (**d**) Observed nuclear structure of $^{29}Si(p,\gamma)^{30}P$, $E_x = 7.446\ MeV$. (**e**) 1.9 MeV H^+ beam radiation of a thick graphite plate. Theoretical photon energy shielding attenuation comparison using 10 mm of Pb as a function of distance.

Fig. 4: (**a**) Decaying radiation from H^+ at 1.1, 1.6, and 1.9 MeV. (**b**) 1100 keV 1000 uA H^+ into four wafer types, measured at 5 cm each time post implant. P-Type, N-Type, Photoresist (PR), and PR with 60 keV $5x10^{15}$ pre-implanted B+. (**c**) Experimental setup. Radiation is measured in the FOUP, with the last wafer (#25) measured post-implant. (**d**) 600 keV 800 μA 10^{15} H+ implant into SiC wafer measured at 5 cm. Experimental $T_{1/2}$ = 647.8 ± 51.8 [sec].

Figure 1:

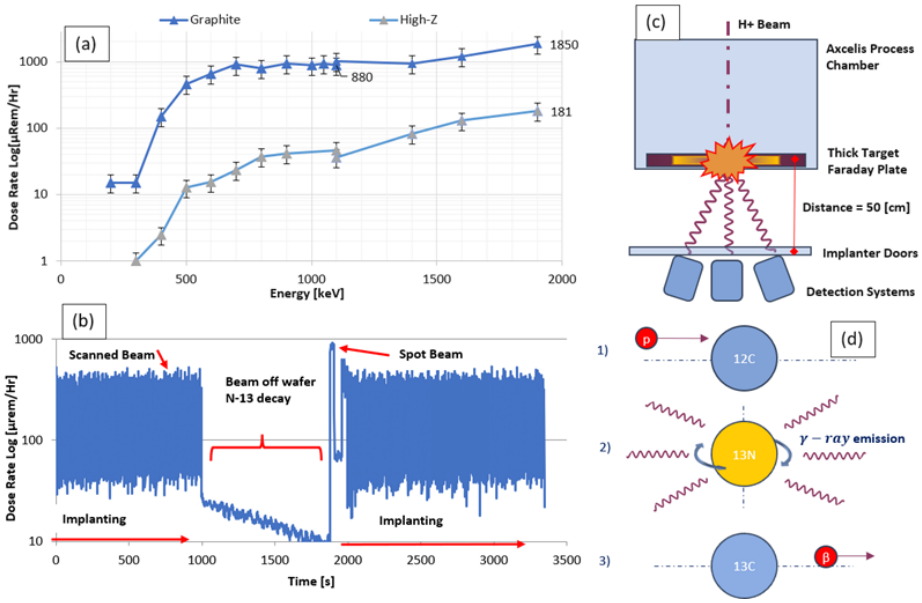

Figure 2:

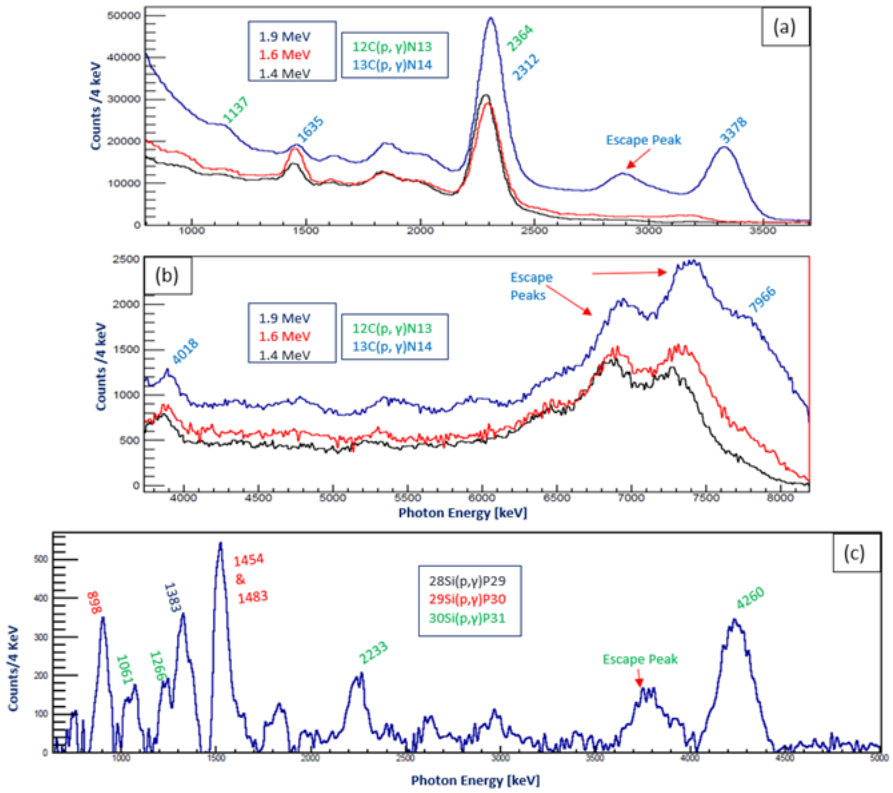

Figure 3:

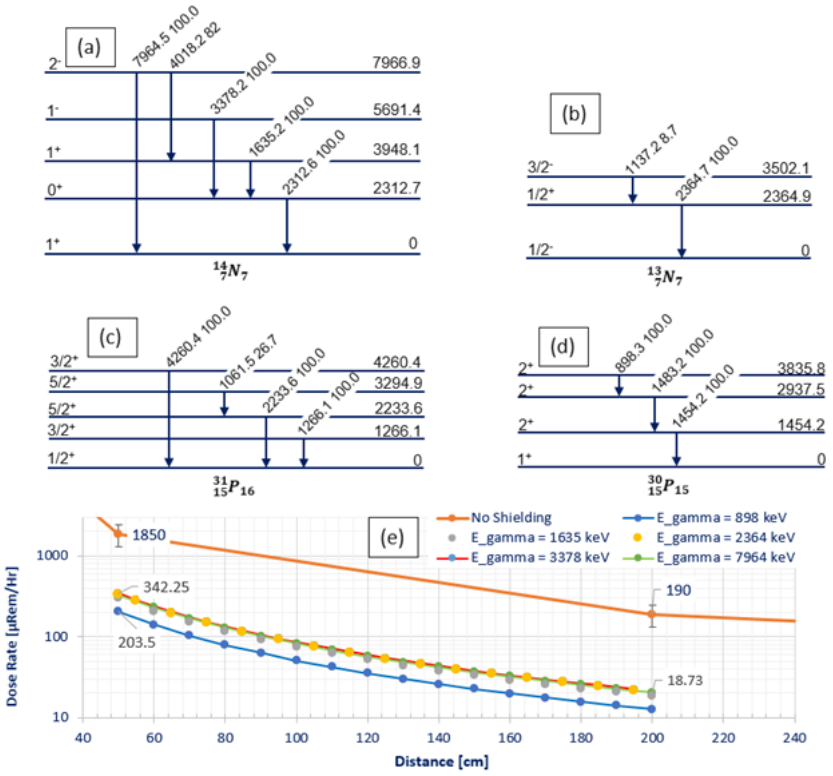
(a)
7964.5 100.0
4018.2 82
3378.2 100.0
1635.2 100.0
2312.6 100.0
2⁻
1⁻
1⁺
0⁺
1⁺
7966.9
5691.4
3948.1
2312.7
0
$^{14}_{7}N_{7}$
(b)
1137.2 8.7
2364.7 100.0
3/2⁻
1/2⁺
1/2⁻
3502.1
2364.9
0
$^{13}_{7}N_{7}$
(c)
4260.4 100.0
1061.5 26.7
2233.6 100.0
1266.1 100.0
3/2⁺
5/2⁺
5/2⁺
3/2⁺
1/2⁺
4260.4
3294.9
2233.6
1266.1
0
$^{31}_{15}P_{16}$
(d)
898.3 100.0
1483.2 100.0
1454.2 100.0
2⁺
2⁺
2⁺
1⁺
3835.8
2937.5
1454.2
0
$^{30}_{15}P_{15}$
(e)
No Shielding
E_gamma = 898 keV
E_gamma = 1635 keV
E_gamma = 2364 keV
E_gamma = 3378 keV
E_gamma = 7964 keV
1850
342.25
203.5
190
18.73
Dose Rate [μRem/Hr]
Distance [cm]
1000
100
10
40
60
80
100
120
140
160
180
200
220
240

Figure 4:

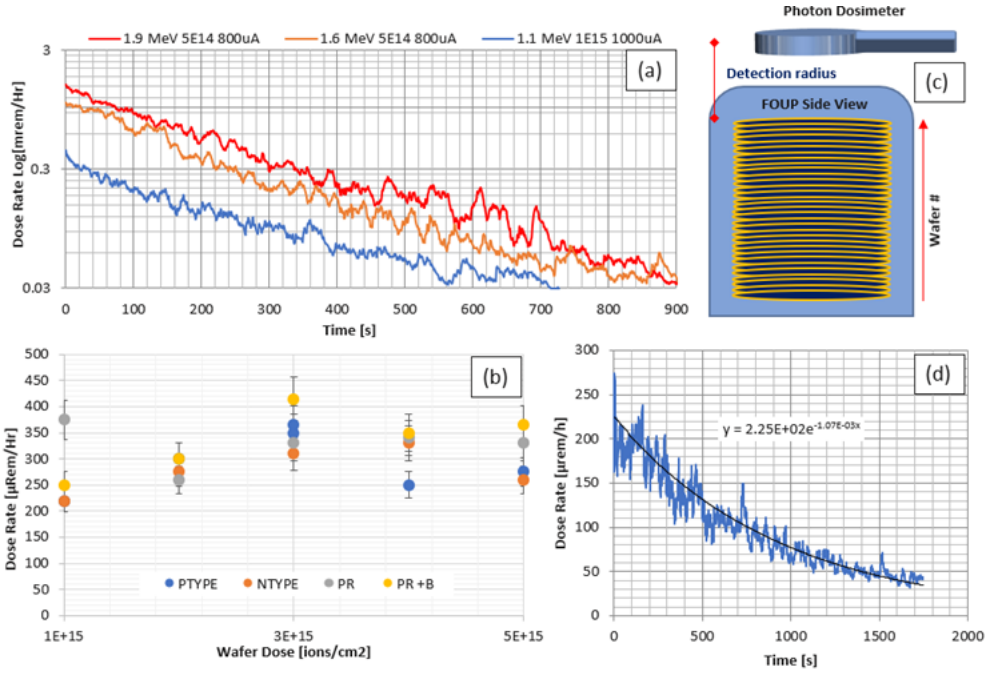
1.9 MeV 5E14 800uA
1.6 MeV 5E14 800uA
1.1 MeV 1E15 1000uA
(a)
Dose Rate Log[mrem/Hr]
Time [s]
Photon Dosimeter
Detection radius
FOUP Side View
(c)
Wafer #
(b)
Dose Rate [µRem/Hr]
PTYPE
NTYPE
PR
PR +B
Wafer Dose [ions/cm2]
(d)
y = 2.25E+02e-1.07E-03x
Dose Rate [µrem/h]
Time [s]